First principles calculations of the σ and χ phases in the Mo–Re and W–Re systems

2010 J. Phys.: Condens. Matter 22 035402

(http://iopscience.iop.org/0953-8984/22/3/035402)

J. Phys.: Condens. Matter **22** (2010) 035402 (7pp) doi:10.1088/0953-8984/22/3/035402

First principles calculations of the σ and χ phases in the Mo–Re and W–Re systems

J-C Crivello and J-M Joubert

ICMPE-CMTR, CNRS UMR-7182, 2-8, rue Henri Dunant, 94320 Thiais, France

E-mail: crivello@icmpe.cnrs.fr

Received 28 August 2009, in final form 1 December 2009
Published 21 December 2009
Online at stacks.iop.org/JPhysCM/22/035402

Abstract

The total energies of all the ordered configurations of the σ and χ phases have been calculated by using first principles methodology in both Mo–Re and W–Re systems. These two complex structures possess 5 and 4 inequivalent sites generating 32 and 16 different ordered configurations, respectively, for a binary A–B system. The converged total energies of all the fully relaxed structures have been used to compute the occupancy of the inequivalent sites as a function of composition and temperature by using the Bragg–Williams approximation in the complete composition range. It is shown that the configurational entropy stabilizes the σ and χ phases in the Mo–Re and W–Re systems. The results evidence the preference of Re for lower coordination number site occupancy and are in very good agreement with the experimental measurements. Tentative *ab initio* phase diagrams have also been drawn.

(Some figures in this article are in colour only in the electronic version)

1. Introduction

In order to increase the creep resistance of the Ni-based superalloys used for very demanding applications such as high temperature gas turbines, refractory elements are added [1]. However, a high concentration of these additive elements leads to the precipitation of topologically close packed (tcp) phases, which are responsible for the depletion of the matrix in the alloying elements, and brittleness. Among the alloying elements used in the third generation superalloys, *molybdenum*, *tungsten* and *rhenium* are particularly important. Mo–Re and W–Re systems exhibit similar phase diagram properties: existence of the same two intermetallic compounds (χ and σ) with similar homogeneity ranges and similar topology (high temperature stability of σ and peritectoid formation of χ). Recent reviews of the experimental data on these two systems and a thermodynamic description using the Calphad method are available [2–4].

In the present work, *ab initio* calculations have been performed for the complete set of ordered configurations generated by distributing A or B elements in the σ and χ phases among the different sites for the two binary A–B systems with $A = \{\text{Mo}, \text{W}\}$ and $B = \text{Re}$. Total energies have been used in order to compute the atomic distribution at finite temperature in the Bragg–Williams (BW) approximation. Comparisons have been made with the available experimental results.

2. Crystal structures

The structure of Frank–Kasper or tcp phases is characterized by the unique presence of tetrahedral interstices, and a limited number of coordination polyhedra. As a result, the crystal structures can be described in terms of networks of intersecting coordination polyhedra [5] with coordination numbers (CN) ranging from 12 to 16. The crystal chemistry of the χ and σ phases has recently been reviewed in detail [6, 7]. These two latter papers focus on the non-stoichiometry of the two compounds in binary systems, showing that it is accommodated by an atomic mixing of the two elements on the different sites of the structure. The change of site occupancies as a function of composition in the different systems has been analyzed and conclusions have been derived in order to define models to be used in the Calphad thermodynamic modeling technique.

2.1. The σ phase

The crystal structure of the σ phase is tetragonal, described by a $P4_2/mnm$ space group (No. 136), with five non-equivalent positions ('s' $= \mathcal{A}, \mathcal{B}, \mathcal{C}, \mathcal{D}, \mathcal{E}$). For a binary compound, the

Table 1. Crystal structure of the σ and χ phases: sites 's', CN, Wyckoff position, and atomic positions (average values). To avoid confusion between different sites with the same Wyckoff notation, the sites are labeled by letters ($\mathcal{A}, \mathcal{B}, \mathcal{C}, \ldots$) for each phase.

	Site 's'	CN	Wyckoff	x	y	z
σ-D8$_b$	$\mathcal{A}$	12	2a	0	0	0
$P4_2/mnm$	$\mathcal{B}$	15	4f	∼0.40	x	0
No. 136	$\mathcal{C}$	14	8i	∼0.46	∼0.13	0
	$\mathcal{D}$	12	8i	∼0.74	∼0.07	0
	$\mathcal{E}$	14	8j	∼0.18	x	∼0.25
χ-A12	$\mathcal{A}$	16	2a	0	0	0
$I\bar{4}3m$	$\mathcal{B}$	16	8c	∼0.32	x	x
No. 217	$\mathcal{C}$	13	24g	∼0.36	x	∼0.04
	$\mathcal{D}$	12	24g	∼0.09	x	∼0.28

distribution of one or the other element on the different sites generates $2^5 = 32$ different ordered configurations. Details of the structure are shown in table 1. Depending on the system, the cell parameters a and c take experimental values from 8.78 to 10.06 Å and 4.55 to 5.23 Å, respectively [6]. The $\mathcal{A}$ and $\mathcal{D}$ sites have a CN of 12, whereas sites $\mathcal{B}, \mathcal{C}$ and $\mathcal{E}$ present a higher CN (14 and 15).

2.2. The χ phase

The χ phase is another important Frank–Kasper phase, which appears in many systems and in which different ordering schemes may be observed, yielding different structure types: αMn, Ti_5Re_{24} and $Mg_{17}Al_{12}$. The space group is $I\bar{4}3m$ (No. 217) and four non-equivalent sites are occupied ($\mathcal{A}, \mathcal{B}, \mathcal{C}, \mathcal{D}$) generating $2^4 = 16$ ordered configurations for a binary compound (see details in table 1). The average cubic cell parameter is about 7.8 Å (from 8.95 to 12.35 Å) [7]. The four different sites define four different coordination spheres with CN12 $\mathcal{D}$, CN13 $\mathcal{C}$ and CN16: $\mathcal{A}$ and $\mathcal{B}$. The presence of a coordination polyhedron of CN13 is an anomaly excluding, in principle, this phase from the Frank–Kasper phase group.

3. Computational details

The density functional theory (DFT) method [8, 9] has been used to perform the calculations in the generalized gradient approximation (GGA) with the Perdew–Wang functional [10] and with projector augmented wave (PAW) pseudo-potentials (PP) [11], as implemented in the Vienna *ab initio* simulation package (VASP) [12, 13]. Convergence tests were performed with respect to the number of plane waves and the k-points mesh. The self-consistent total energy calculations converged to less than 0.1 meV, with a 350 eV cutoff energy and with k-points spacing less than 0.06 Å^{-1} in each direction, with samplings generated by the Monkhorst–Pack procedure [14]. For the σ and χ-phases, it corresponds, respectively, to a grid of $8 \times 8 \times 15$ and $10 \times 10 \times 10$ points in the irreducible wedge of the Brillouin zone. Both the internal atomic coordinates and the lattice parameters were fully relaxed. For all the configurations, relaxations was performed to converge to a maximum Hellmann–Feynman force of less than 5 meV Å^{-1} for each configuration close to the convex hull, and less than 10 meV Å^{-1} for the other configurations, since the latter have no significant effect on the calculated site occupancy and energy as a function of composition. Total energies have been calculated using the linear tetrahedron method with Blöchl corrections [15]. Only electronic contributions to the total energy are included at 0 K, i.e. vibrational and electronic entropies were not considered.

Finite temperature thermodynamic properties were modeled in the Bragg–Williams (BW) approximation, with no excess terms [16]. Considering that the only contribution to the entropy is the atomic mixing on the different sites, the Gibbs energy of the phase is given by

$$G = G^{\text{ref}} - T * S^{\text{mixing}} + G^{\text{excess}}, \qquad G^{\text{excess}} = 0. \quad (1)$$

The Gibbs energy surface of reference is expressed by

$$G^{\text{ref},\sigma} = \sum_{ijklm} [y_i^{(\mathcal{A})} y_j^{(\mathcal{B})} y_k^{(\mathcal{C})} y_l^{(\mathcal{D})} y_m^{(\mathcal{E})}] * H^{0,\sigma}_{ijklm}$$
$$G^{\text{ref},\chi} = \sum_{ijkl} [y_i^{(\mathcal{A})} y_j^{(\mathcal{B})} y_k^{(\mathcal{C})} y_l^{(\mathcal{D})}] * H^{0,\chi}_{ijkl}, \quad (2)$$

where G^{ref} is the sum of the formation enthalpies $H^{0,\chi(\sigma)}_{ijkl(m)}$ of all the configurations $ijkl(m)$ with a single species $i = \{\text{Mo, W}\}$ or Re, on each site s, weighted by the product of site fractions $y_i^{(s)}$. The formation enthalpies are calculated by subtracting the total energy E and the energy of the equivalent amount of the elements in their standard element reference (SER) states, bcc for A elements (Mo, W) and hcp for B (Re):

$$H^{\chi(\sigma)}_{ijkl(m)} = E^{\chi(\sigma)}_{ijkl(m)} - x_{\text{A}} * E^{\text{bcc}}_{\text{A}} - x_{\text{B}} * E^{\text{hcp}}_{\text{B}}, \quad (3)$$

with x_i the mole fraction of the i element. The ideal entropy of mixing is expressed as

$$S^{\text{mixing}} = -R \sum_s a^{(s)} \sum_{i=A,B} y_i^{(s)} * \ln(y_i^{(s)}), \quad (4)$$

where R is the gas constant and $a^{(s)}$ is the multiplicity of site s, as given in table 1. The calculations, consisting of Gibbs energy minimization to find the most stable distribution of the elements, were performed in the Thermo-Calc software [17].

4. Results

The calculated heats of formation are listed in table 2 and displayed in figure 1. Convergence to a stable structure was observed for each σ and χ configuration in Mo–Re and W–Re systems. The distribution of the energies is quite similar between the two A–B systems. The convex hull is shown. The minimum enthalpy of the σ-phase is found for the configuration ReAReReA in the Mo–Re system and ReAAReA for the W–Re system, and the energies of these two configurations are very close. For the χ phase, the minimum is always found for the configuration AAReRe (stoichiometry A_5B_{24}). Systematically, when different configurations give rise to the same compositions, lower values of the enthalpy are observed when Re occupies the sites of lower coordination, demonstrating the preference of this element for these sites. No configuration of the σ phase presents a negative value of

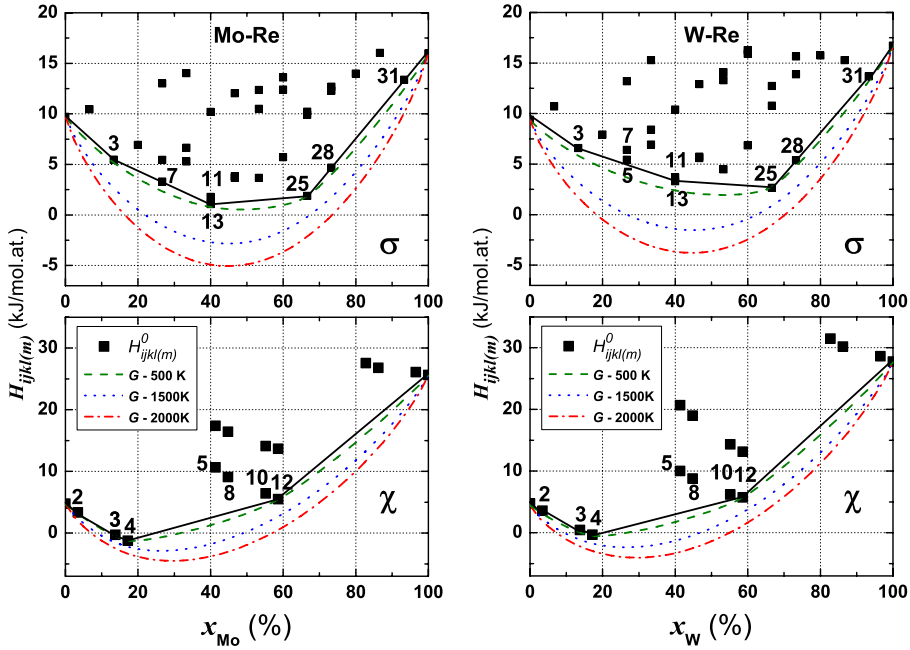

Figure 1. Formation enthalpies $H^{0,\chi(\sigma)}_{ijkl(m)}$ (kJ/mol.-at.) of all $ijkl(m)$ configurations with a single species i = Mo or Re (left) and i = W or Re (right) as a function of x_A, in σ (upper) and χ (lower) structures, with respect to the elemental groundstates. The most stable configurations have been connected with a solid line. Numbers refers to No. of the most significant configurations (table 2). Gibbs free energies obtained in the BW approximation are also displayed at 500 K (dash line), 1500 K (dots) and 2000 K (dash dot line).

the formation enthalpy. The phase is therefore predicted to be unstable at 0 K as regards decomposition into the pure elements and it can be anticipated that a strong contribution of the configurational entropy is needed to stabilize it at finite temperatures. On the contrary, negative values of the formation enthalpies corresponding to the configurations ReAReRe and AAReRe for the χ phase are observed. As we will see, this is in perfect agreement with the phase diagram.

The full relaxation of both the lattice parameters and the internal atomic positions was performed. For both structures, a linear increase of the cell volume is observed as a function of x_A, as predicted by the Vegard's law and the relative atomic sizes. For the tetragonal σ phase, the average relaxed c/a ratio is 0.524, and slightly lower values are observed for the most stable compounds. The relaxed atomic positions are similar, whatever the system and the configuration, to within 0.003. This is in agreement with the results of Berne *et al* [2], that shows the internal relaxation has no significant effect on the formation energy. Additionally, considering the errors from the exchange–correlation functional approximation, the average coordinates are consistent with the average experimental values (to within 0.005) [6, 7].

5. Discussion

5.1. Site occupancies

The computed inequivalent site occupancies of the A element at moderate temperature (500 K), obtained from the *ab initio* results treated in the BW approximation, are shown in figure 2. In agreement with the relative similarity of the calculated formation enthalpies, the results are similar for the two studied systems. For both phases, the occupancy sequence clearly indicates that the element A has a preference for higher CN sites. In the σ phase, element A first occupies only the CN15 site, $\mathcal{B}$. Increasing the A content, element A replaces Re on the two $(\mathcal{E}, \mathcal{C})$-CN14 sites with comparable filling tendency. Finally, at a high A concentration, A replaces Re on the two sites $(\mathcal{A}, \mathcal{D})$-CN12 simultaneously. A comparable behavior is found for the χ phase. First, Re is replaced by A on the two sites $(\mathcal{A}, \mathcal{B})$-CN16 simultaneously, then on site $\mathcal{C}$-CN13 and finally on site $\mathcal{D}$-CN12. At this temperature, the atomic distribution is more ordered in the χ phase than in the σ phase due to a smaller complexity and a smaller number of configurations in, or close to, the convex hull.

At higher temperature (1873 K, figure 3), the general tendency of the occupancy sequence is similar to that observed at 500 K. The effect of temperature is to increase the amount of atomic mixing because the contribution of the entropy to the Gibbs energy becomes higher. At this chosen temperature, experimental site occupancies are available [6, 7] and they compare astonishingly well with the computed values. Site occupancies as a function of temperature have been calculated for two Mo–Re composition: σ-$Mo_{30}Re_{70}$ and χ-$Mo_{23}Re_{77}$ (figure 4). Again, experimental site occupancies are shown and are in very good agreement with the calculated data. The disagreement is larger in the χ phase for the sites of low multiplicity $(\mathcal{A}, \mathcal{B})$, because the experimental error is larger on these sites [4]. It is interesting to compare the two phases as regards the evolution of the level of order. The χ phase remains very ordered below 1000 K and then, progressively, accepts atomic mixing, while the σ phase presents a higher degree of atomic mixing at low temperatures which changes more smoothly when the temperature increases. Both phases

Table 2. Calculated formation enthalpy for all the calculated A–Re configurations ($A = \{\text{Mo, W}\}$) in σ (left) and χ (right) structures. As indicated: number of configuration (No.), composition of A element (x_a in %), $ijkl(m)$ configuration, calculated formation enthalpy $H^{0,\chi(\sigma)}_{ijkl(m)}$ (kJ/mol.-at.), volume and c/a ratio for σ structures. The most stable configurations are shown in bold characters. The total energy and lattice parameters of pure elements are indicated for the bcc and hcp structure.

			A = Mo			A = W						A = Mo		A = W	
No.	x_A	σ-$ijklm$	H^{σ}_{ijklm}	vol (Å^3)	c/a	H^{σ}_{ijklm}	vol (Å^3)	c/a	No.	x_A	χ-$ijkl$	H^{χ}_{ijkl}	vol (Å^3)	H^{χ}_{ijkl}	vol (Å^3)
1	00.0	ReReReReRe	**09.37**	456.67	0.524	—	—	—	1	00.0	ReReReRe	**04.76**	442.07	—	—
2	06.7	AReReReRe	10.44	456.94	0.529	10.70	458.26	0.528	2	03.4	AReReRe	**03.33**	442.86	**03.58**	442.84
3	13.3	ReAReReRe	**05.48**	458.52	0.525	**06.59**	459.36	0.522	3	13.8	ReAReRe	**−00.30**	444.99	**00.44**	445.38
4	20.0	AAReReRe	06.92	459.77	0.527	07.91	461.55	0.524	4	17.2	AAReRe	**−01.26**	445.87	**−00.31**	446.12
5	26.7	ReReAReRe	05.44	461.04	0.523	**05.43**	463.35	0.521	5	41.4	ReReARe	**10.63**	452.21	**10.01**	455.19
6	26.7	ReReReARe	13.01	461.05	0.529	13.19	464.64	0.530	6	41.4	ReReReA	17.39	454.99	20.67	454.99
7	26.7	ReReReReA	**03.30**	459.43	0.511	06.40	462.69	0.520	7	44.8	AReReA	16.44	456.02	18.98	456.02
8	33.3	AReAReRe	06.65	462.18	0.525	**06.92**	465.54	0.523	8	44.8	AReARe	**09.08**	457.28	**08.77**	456.00
9	33.3	AReReARe	14.03	461.17	0.531	15.28	466.82	0.532	9	55.2	ReAReA	14.11	454.83	14.33	459.03
10	33.3	AReReReA	**05.29**	460.76	0.513	08.41	465.11	0.521	10	55.2	ReAARe	**06.42**	457.84	**06.21**	458.55
11	40.0	ReAAReRe	01.78	463.97	0.524	03.69	467.05	0.520	11	58.6	AAReA	13.66	460.13	13.14	460.13
12	40.0	ReAReARe	10.29	463.85	0.526	10.39	468.49	0.526	12	58.6	AAARe	**05.51**	456.26	**05.71**	459.55
13	40.0	ReAReReA	**01.07**	463.05	0.511	**03.31**	466.77	0.518	13	82.8	ReReAA	27.55	458.99	31.46	470.20
14	46.7	AAAReRe	**03.69**	465.32	0.526	**05.58**	469.38	0.522	14	86.2	AReAA	26.78	460.26	30.17	471.22
15	46.7	AAReARe	12.03	465.04	0.530	12.91	470.53	0.528	15	96.6	ReAAA	26.11	462.63	28.63	474.38
16	46.7	AAReReA	03.80	464.49	0.513	05.73	469.19	0.520	16	100.0	AAAA	**25.64**	464.16	**27.74**	475.43
17	53.3	ReReAARe	12.36	466.37	0.529	14.08	472.28	0.528							
18	53.3	ReReReAA	10.50	464.94	0.518	13.28	471.92	0.525							
19	53.3	ReReAReA	**03.67**	466.01	0.514	**04.48**	471.20	0.520							
20	60.0	AReAARe	13.60	467.46	0.532	16.27	474.50	0.530							
21	60.0	AReReAA	12.39	465.83	0.520	15.93	474.49	0.526							
22	60.0	AReAReA	**05.71**	467.26	0.516	**06.85**	473.64	0.521							
23	66.7	ReAAARe	10.22	469.82	0.528	12.72	476.34	0.525							
24	66.7	ReAReAA	09.91	468.93	0.517	10.78	476.01	0.524							
25	66.7	ReAAReA	**01.88**	469.93	0.514	**02.64**	475.09	0.519							
26	73.3	AAAARe	12.30	471.02	0.530	15.63	478.55	0.526							
27	73.3	AAReAA	12.68	470.33	0.520	13.88	478.37	0.525							
28	73.3	AAAReA	**04.67**	471.20	0.516	**05.39**	477.63	0.521							
29	80.0	ReReAAA	13.98	471.82	0.520	15.74	480.73	0.526							
30	86.7	AReAAA	16.02	472.96	0.524	15.28	483.16	0.527							
31	93.3	ReAAAA	**13.36**	476.75	0.522	**13.68**	485.83	0.523							
32	100.0	AAAAA	**15.97**	478.15	0.524	**16.71**	487.22	0.524							

Pure elements

Elt.	Struc.	E_i^{struc} (eV/at.)	a (Å)	c/a
Mo	bcc	**−10.911**	3.153	—
	hcp	−10.475	2.748	1.781
W	bcc	**−12.919**	3.175	—
	hcp	−12.420	2.769	1.785
Re	bcc	−12.029	3.114	—
	hcp	**−12.348**	2.781	1.610

remain ordered far below 3000 K. The disordered behavior of the Mo site occupancy at low temperature is attributed to the effect of configurations very close to the convex hull, the influence of which changes dramatically with temperature.

5.2. Phase diagrams

The *ab initio* calculated binary phase diagrams of the two systems are shown in figure 5. They have been calculated from the calculated formation enthalpies on σ and χ phases (table 2) using the BW approximation. With first principles calculations, we have not calculated the thermodynamic properties of the terminal bcc and hcp solid solution phases and we have neglected any interaction in these phases. The liquid phase has not been introduced either. The peritectoid hcp$+\sigma \Leftrightarrow \chi$ transformation is not found and the homogeneity ranges of some of the phases is not very well reproduced; this may be attributed to the poor description of the solid solution phases. Nevertheless, the essential features of the topology are reproduced, such as the stability at low temperature of the χ phase and the eutectoid decomposition of σ, confirmed experimentally in the Mo–Re systems [4]. It is predicted in the present work for W–Re system, but may be very difficult to evidence experimentally given the slow reaction rate at these temperatures.

5.3. Calphad modeling

The Calphad method is a powerful semi-empirical method dedicated to the description of the thermodynamic properties of phases and compounds. One of the main applications is the calculation of multi-component phase equilibria and phase diagrams. To model simple systems, such as binary systems, models should be defined adequately with the thermodynamic and structural properties of the phase. These models have parameters which are assessed to describe the available experimental data. For non-stoichiometric compounds, the so-called sublattice model, as expressed in the compound energy formalism, is commonly used [18]. To define the equations giving the Gibbs energy of the phase, one should know the mechanism responsible for the non-stoichiometry, in particular, the site multiplicity of the sites on which atom or

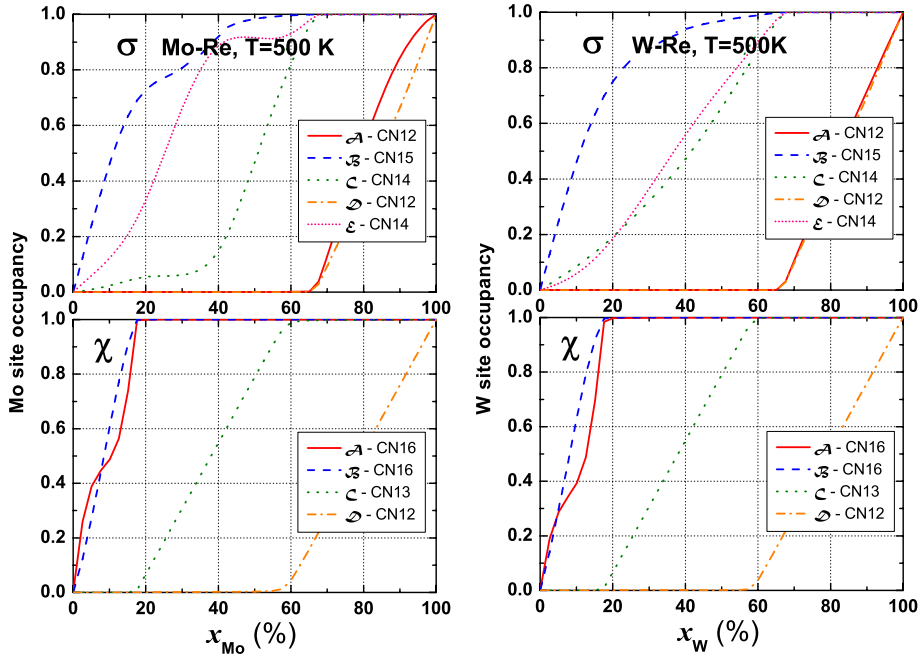

Figure 2. Computed occupancy at 500 K on the different sites as a function of composition x_A, for σ (upper) and χ (lower) Mo–Re (left) and W–Re (right) systems. Re fills each site not fully occupied by A.

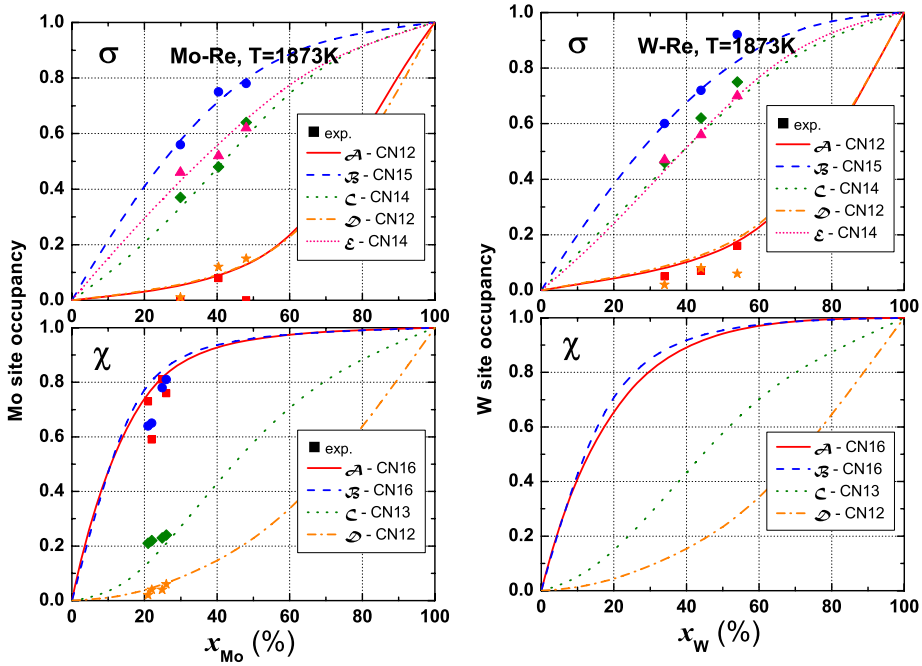

Figure 3. Computed occupancy at 1873 K on the different sites as a function of composition x_A, for σ (upper) and χ (lower) Mo–Re (left) and W–Re (right) system. Re fills each site not fully occupied by A. Experimental site occupancies [2, 6, 7], are shown for comparison, on $\mathcal{A}$—● $\mathcal{B}$—■ $\mathcal{C}$—♦ $\mathcal{D}$—★ $\mathcal{E}$—▲ sublattices.

vacancy mixing is present. Then, some simplifications should be made in order to limit the number of parameters while conserving a correct evaluation of the configurational entropy.

The models used for σ and χ phases have recently been reviewed [6, 7] and new proposals have been made, based on a careful analysis of the site occupancies as a function of composition in a large number of systems. For the σ phase, contrary to previous models, it was proposed that, in a first approximation, the three sites of high CN, on the one hand, and the two sites of low CN, on the other hand, could be grouped together because their occupancy is not very different [6]. This yields the following model: $(A, B)_{20}^{\mathcal{BCE}}(A, B)_{10}^{\mathcal{AD}}$. The power of the *ab initio* calculation is to offer a complete picture of a given system in the whole composition range, as presented

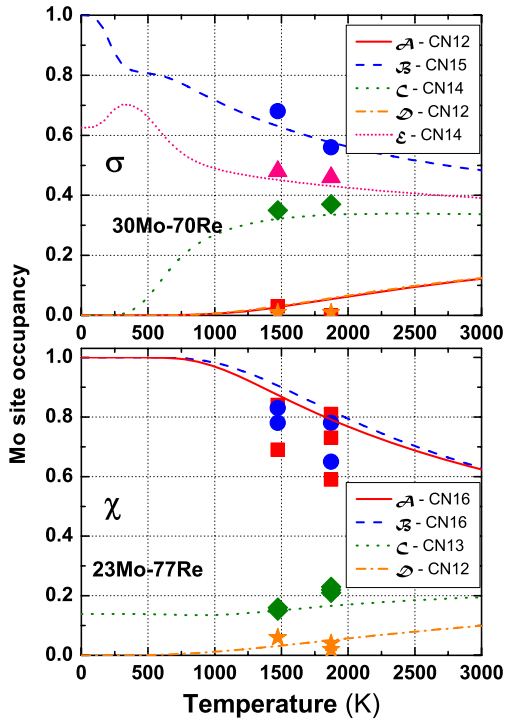

Figure 4. Computed site occupancy as a function of temperature, on each sublattice of two Mo–Re compounds: σ-$Mo_{30}Re_{70}$ (upper) and χ-$Mo_{23}Re_{77}$ (lower). Experimental site fractions on $\mathcal{A}$—● $\mathcal{B}$—■ $\mathcal{C}$—♦ $\mathcal{D}$—★ $\mathcal{E}$—▲ sublattices, are shown for comparison for σ-$Mo_{29.9}Re_{70.1}$, σ-$Mo_{31.9}Re_{68.1}$, χ-$Mo_{22}Re_{78}$, χ-$Mo_{21}Re_{79}$, χ-$Mo_{23}Re_{77}$, χ-$Mo_{24.9}Re_{75.1}$ [6, 7].

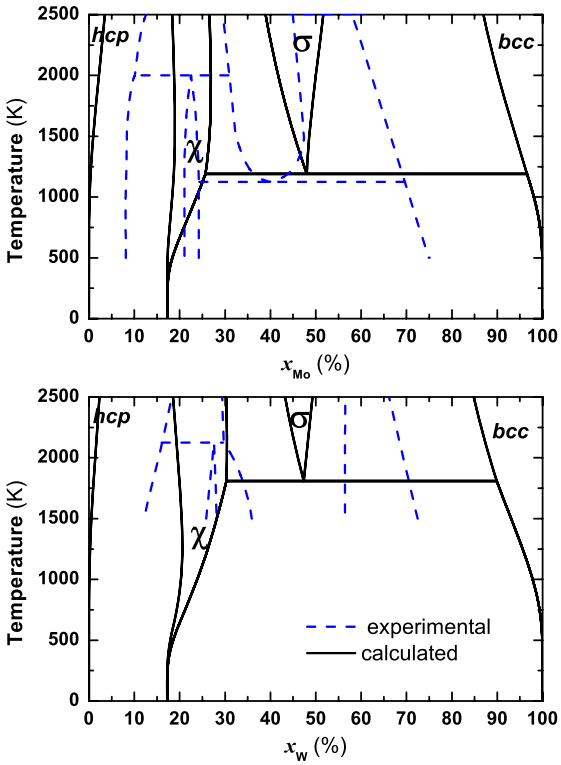

Figure 5. *Ab initio* calculated binary phase diagrams of Mo–Re (upper) and W–Re (lower) system, computed in the BW approximation. Experimental phase diagrams (dash line) are shown for comparison.

in figures 2 and 3, while only the stable homogeneity range of the phase is available experimentally. These two figures demonstrate the quality of the proposed model, especially at high temperatures for which the phase is stable and at which the site occupancy on site $\mathcal{A}$ approaches that of sites $\mathcal{C}$ and $\mathcal{E}$.

For the χ phase, the model $(A, B)^{\mathcal{AB}}_{10}(A, B)^{\mathcal{C}}_{24}(A, B)^{\mathcal{D}}_{24}$ has been proposed [7], corresponding to the grouping of the sites of the same CN in the same sublattices. The sequential occupation of the different sites by A, as observed in figures 2 and 3, is in complete agreement with this formalism.

5.4. Comparison with other studies

Owing to the increasing performance of supercomputers and the availability of relatively inexpensive high performance workstations, several systematic studies of complex structures have been performed using first principles techniques. In the case of the σ phase, the complete configuration sets have been calculated with the DFT-method using different approximations, e.g. Fe–Cr in the Linear muffin-tin orbital-atomic-sphere approximation (LMTO-ASA) [19], Co–Cr in the full potential linearized augmented plane wave (FLAPW) method [20], and Mo–Ru with PP [21].

Concerning the systems studied in the present work, two studies in the PP method are available. Hammerschmidt *et al* [22], have shown the convex hull in the σ and χ phases in both Mo–Re and W–Re systems. Berne *et al* [2] have calculated all the configurations of the σ phase in the W–Re system and site occupancies by the Connolly–Williams method using a cluster variation method (CWM–CVM). Our results are in fair agreement with both studies, given the different approximations and calculation parameters used.

These latter *ab initio* results have also been used by [23] to compute the site occupancies in the BW approximation, with similar results. In the present work, we confirm that this much simpler approach, compared to CWM–CVM, is sufficient to compute the finite temperature properties for the two systems Mo–Re and W–Re.

The χ phase has not been subject to a complete study of all the configurations in any system. As far as we know, only one comparable first principles study is available in the Mg–Al system [24], though only half of the configurations were computed (2a and 8c are considered to have the same occupancy). The calculations suggest the same behavior as we have found: the smaller atom (Al) presents a preferential occupancy for lower CN sites, the larger (Mg) for higher CN sites (see [7] for a computation of site occupancies done after these calculations).

6. Conclusions

We have presented a complete description of the two complex σ and χ phases in the Mo–Re and W–Re systems based on first principles calculations. After structural relaxation of all the ordered configurations, enthalpies of formation, lattice stability and atomic coordinates have been analyzed.

These results illustrate that the A = {Mo, W} element has a preference for higher CN sites, whereas the smaller atom (B = Re) presents a preferential occupancy for lower CN sites, in agreement with the experimental measurements. Concerning the description of site occupancies as a function of composition, our conclusions agree with the conclusions obtained previously for the Calphad description of both σ and χ phases [6, 7]. The excellent agreement obtained between computed and experimental site occupancies, and the relative agreement of phase diagram calculations, demonstrates the efficiency of the BW approximation, in spite of its simplicity compared to CVM, for the computation of finite temperature thermodynamic properties. For both Mo–Re and W–Re systems, it is shown that the configurational entropy stabilizes the two complex χ and σ phases with certain homogeneity ranges.

Acknowledgment

This work was performed using HPC resources from GENCI-CINES (Grants 2009-096175).

References

[1] Reed R C 2008 *The Superalloys: Fundamentals and Applications* (Cambridge: Cambridge University Press)
[2] Berne C, Sluiter M H F, Kawazoe Y, Hansen T and Pasturel A 2001 Site occupancy in the Re–W σ phase *Phys. Rev.* B **64** 144103
[3] Mao P, Han K and Xin Y 2008 Thermodynamic assessment of the Mo–Re binary system *J. Alloys Compounds* **464** 190–6
[4] Farzadfar S, Levesque M, Phejar M and Joubert J-M 2009 Thermodynamic assessment of the molybdenum–rhenium system *Calphad* at press
[5] Sinha A 1972 Topologically close-packed structures of transition metal alloys *Prog. Mater. Sci.* **15** 79–185
[6] Joubert J-M 2008 Crystal chemistry and calphad modeling of the σ phase *Prog. Mater. Sci.* **53** 528–83
[7] Joubert J-M and Phéjar M 2009 Crystal chemistry and calphad modeling of the χ phase *Prog. Mater. Sci.* **54** 945–1058
[8] Hohenberg P and Kohn W 1964 Inhomogeneous electron gas *Phys. Rev.* **136** B864–71
[9] Kohn W and Sham L J 1965 Self-consistent equations including exchange and correlation effects *Phys. Rev.* **140** A1133–40
[10] Perdew J P and Wang Y 1992 Accurate and simple analytic representation of the electron–gas correlation energy *Phys. Rev.* B **45** 13244–9
[11] Kresse G and Joubert D 1999 From ultrasoft pseudopotentials to the projector augmented-wave method *Phys. Rev.* B **59** 1758
[12] Kresse G and Hafner J 1993 *Ab initio* molecular dynamics for liquid metals *Phys. Rev.* B **47** 558–61
[13] Kresse G and Furthmüller J 1996 Efficiency of *ab initio* total energy calculations for metals and semiconductors using a plane-wave basis set *Comput. Mater. Sci.* **6** 15–50
[14] Monkhorst H and Pack J 1976 Special points for Brillouin-zone integrations *Phys. Rev.* B **13** 5188–92
[15] Blöchl P E, Jepsen O and Andersen O K 1994 Improved tetrahedron method for Brillouin-zone integrations *Phys. Rev.* B **49** 16223
[16] Dupin N, Fries S G, Joubert J-M, Sundman B, Sluiter M H F, Kawazoe Y and Pasturel A 2006 Using first-principles results to calculate finite-temperature thermodynamic properties of the Nb-Ni μ phase in the Bragg–Williams approximation *Phil. Mag.* **86** 1631–41
[17] Sundman B, Jansson B and Andersson J-O 1985 The thermo-calc databank system *Calphad* **9** 153–90
[18] Sundman B and Ågren B J 1981 A regular solution model for phases with several components and sublattices, suitable for computer applications *J. Phys. Chem. Solids* **42** 297–301
[19] Sluiter M H F, Esfarjani K and Kawazoe Y 1995 Site occupation reversal in the Fe–Cr-σ phase *Phys. Rev. Lett.* **75** 3142–5
[20] Houserová J, Vřeštál J, Friák M and Šob M 2002 Phase diagram calculation in Co–Cr system using *ab initio* determined lattice instability of σ phase *Calphad* **26** 513–22
[21] Grånäs O, Korzhavyi P, Kissavos A and Abrikosov I 2008 Theoretical study of the Mo–Ru σ phase *Calphad* **32** 171–6
[22] Hammerschmidt T, Seiser S, Drautz R and Pettifor D 2008 Modelling topologically close-packed phases in superalloys: valence-dependent bond-order potentials based on *ab initio* calculations *Superalloys 2008: Proc. TMS Int. Conf., Champion, USA* pp 847–53 edited by TMS (The Minerals, Metals and Materials Society)
[23] Fries S G and Sundman B 2002 Using Re–W σ-phase first-principles results in the Bragg–Williams approximation to calculate finite-temperature thermodynamic properties *Phys. Rev.* B **66** 012203
[24] Zhong Y, Yang M and Liu Z K 2005 Contribution of first-principles energetics to Al–Mg thermodynamic modeling *Calphad* **29** 303–11